Rev.Adv.Mater.Sci. 18(2008) 149-153

ELECTROCHEMICAL BEHAVIOR OF A $Fe_{48}Cr_{15}Mo_{14}Er_2C_{15}B_6$ BULK-METALLIC GLASS

D. C. Qiao, B. Green, M. Morrison and P. K. Liaw

Department of Materials Science and Engineering, University of Tennessee, Knoxville, TN 37996-0100, USA

Received: March 29, 2008

Abstract. Cyclic-anodic-polarization experiments were conducted on a $Fe_{48}Cr_{15}Mo_{14}Er_2C_{15}B_6$ in 1 N HCl, 1 N NaOH, and 0.6 M NaCl with pH of 7. The corrosion-penetration rates (CPRs) in HCl, NaOH, and NaCl are 39.9 μm/year, 27.5 μm/year, and 3.02 μm/year, respectively, indicating good corrosion properties in different environments. The corrosion process is similar in the three different solutions, which was analyzed by the electrochemical-impedance spectroscopy (EIS) in the 0.6 M NaCl solution. The change of the electrode resistance is in agreement with the variation of the polarization curve.

1. INTRODUCTION

The Fe-based bulk metallic glasses (BMGs) have been reported to exhibit high yield strengths two or three times greater than those of high-strength steels and elastic moduli comparable to those of super-austenitic steel alloys [1-3]. These Fe-based BMGs are beginning to gain the recognitions as a new class of structural materials with excellent mechanical and magnetic properties as well as the potential ability to be fabricated to a near-net shape [4-6]. On the other hand, applications of the Fe-based BMGs require a high chemical stability in various environments in order to ensure an acceptable lifetime. If superior electrochemical properties were combined with excellent mechanical properties and good glass-forming abilities, Fe-based BMGs could be interesting candidates for structural and functional applications. It is of importance scientifically and technically to investigate the corrosion behaviors of these amorphous alloys. In this paper, $Fe_{48}Cr_{15}Mo_{14}Er_2C_{15}B_6$ BMG specimens were used for corrosion investigation in 1 N HCl, 1 N NaOH, and 0.6 M NaCl with *p*H of 7 solutions, respectively.

2. EXPERIMENTAL PROCEDURES

The $Fe_{48}Cr_{15}Mo_{14}Er_2C_{15}B_6$ alloys were obtained by melting appropriate amounts of Fe (99.9%), Cr (99.99%), Mo (99.99%), Er (99.9%), C (99.99%), and B (99.99%) in an arc furnace under an argon gas. BMGs specimens were prepared by the suction of the molten alloys into a copper mold. The specimens of BMGs with 3 mm × 3 mm square bars were cut for the X-ray and corrosion experiments by electrical-discharge machining (EDM). X-ray results show that the specimens for all the corrosion measurement are amorphous.

The corrosion behaviors were studied by electrochemical measurements (Princeton Applied Research 263 A potentiostat with Powersuit software) [7]. The specimens were coated with an epoxy resin, except for a measurement area of 0.141 cm^2. Prior to electrochemical measurements, the specimens were mechanically polished with a silicon carbide paper up to No. 600, degreased in acetone, washed in distilled water, and dried in the air. The electrolyte was a 1 N HCl, 1 N NaOH, or 0.6 M NaCl with *p*H of 7 solutions. Electrochemical measurements were conducted in a three-elec-

Corresponding author: P. K. Liaw, e-mail: pliaw@utk.edu

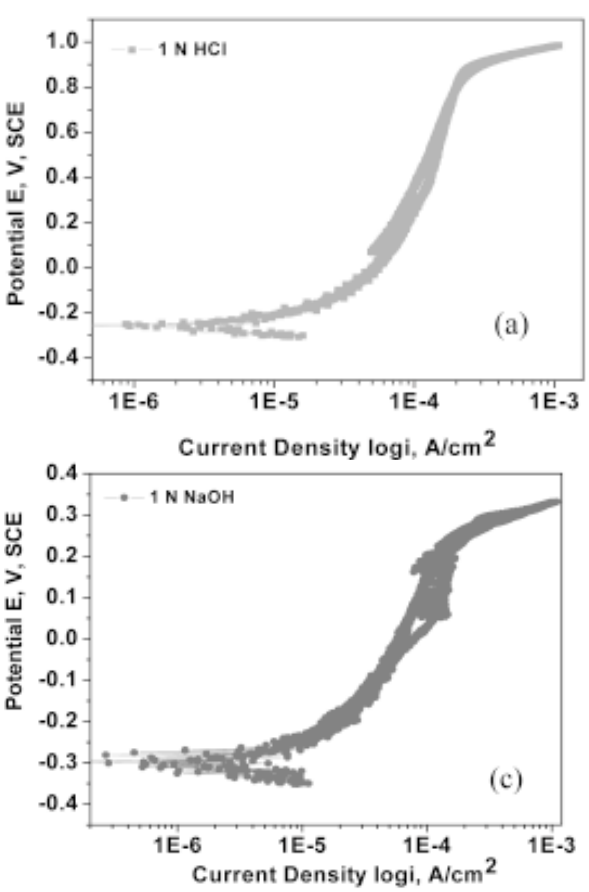

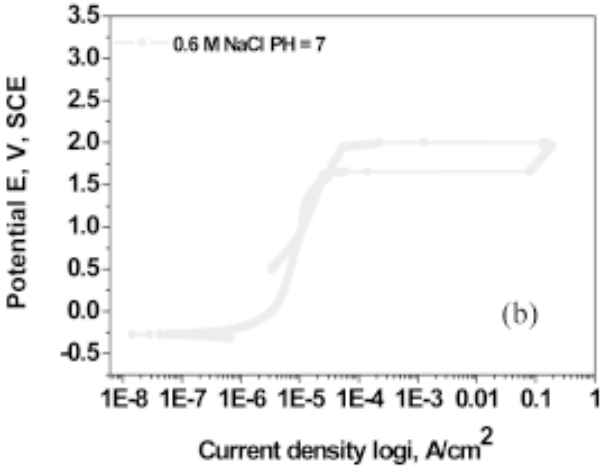

Fig. 1. The cyclic-anodic polarization of the Fe48Cr15Mo14Er2C15B6 in different solutions. (a) 1 N HCl, (b) 0.6 M NaCl, *p*H = 7, and (c) 1 N NaOH.

trode cell using a platinum counter electrode, a saturated calomel reference electrode (SCE), and a working electrode (corrosion specimen). Thus, all potential cited in this paper will henceforth be in reference to the saturated calomel electrode [8,9].

Before each test was initiated, the sample was allowed to stabilize in the electrolyte until the open-circuit corrosion potential ($E_{corr.}$). For cyclic-anodic-polarization experiments, the scan was started at 50 mV below $E_{corr.}$ and continued in the positive direction at a scan rate of 0.17 mV/s until an anodic current density (i) of 10^4 mA/m^2 was reached [10,11]. At this point, the scan direction was reversed, and the potential was decreased at the same rate until the starting potential was reached.

3. RESULTS AND DISCUSSIONS

3.1. Cyclic-anodic-polarization

The cyclic-anodic-polarization curves of the $Fe_{48}Cr_{15}Mo_{14}Er_2C_{15}B_6$ BMG in different solutions are shown in Fig. 1. These three polarization curves show that the corrosion processes in different solutions are very similar, including that the anode dissolves actively, the passive films form, the transpassive phenomenon occurs in 1 N HCl (Fig. 1a) and 1 N NaOH (Fig. 1c), or the pitting phenomenon occurs in 0.6 M NaCl (Fig. 1b), which is proved by the change of the current density and the optical microscopy.

The value of $i_{corr.}$ (the current density at the open circuit) can be calculated by fitting the experimental data to the following Tafel equation used as a theoretical model for the current-potential relationship.

$$i = i_{corr.}\left[10^{(E-E_{corr.})/b_a} - 10^{-(E-E_{corr.})/b_c}\right], \quad (1)$$

where, i is the current density, E is the potential, $E_{corr.}$ is the potential at an open circuit, b_a is the slope of the anode polarization curve, and b_c is the minus slope of the cathode polarization curve.

The R_p is determined as the inverse of the slope according to the current-potential data at the potential where the net current is zero,

$$R_p = \left(\frac{\partial E}{\partial i}\right)_{E_{corr}}, \quad (2)$$

where R_p is the polarization resistance, and $\left(\partial E / \partial i\right)_{E_{corr}}$ is the potential gradient at $E_{corr.}$. R_p is inversely proportional to the corrosion rate.

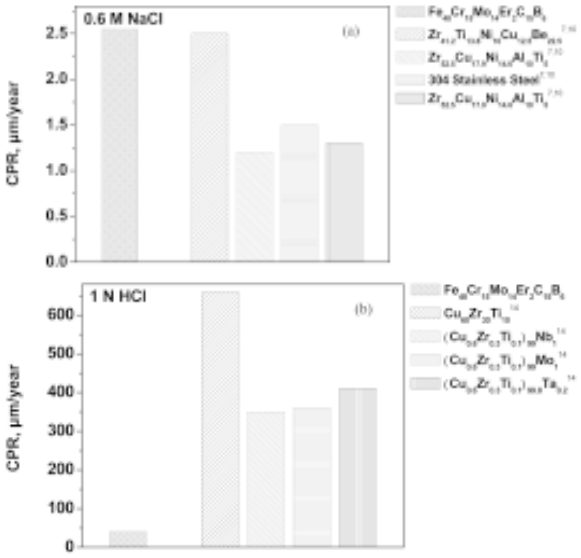

Fig. 2. The CPR of different materials in different solutions. (a) 0.6 M NaCl and (b) 1 N HCl.

$$i_{corr} = \frac{1}{\ln 10}\frac{b_a b_c}{b_a + b_c}\frac{1}{R_p}. \quad (3)$$

The corrosion-current density is a measure of how fast a material is corroding. The corrosion-penetration rate (CPR) is calculated by Faraday's Law [12], which is related to the corrosion-current density.

$$CPR = 0.327(Mi_{corr}) / m\rho, \quad (4)$$

where, M is the atom-fraction-weighted value of the atomic weight (g/mol), and m is the ion valence, and ρ is the density [13,14].

According to the polarization curves and Eqs. (1) – (4), the CPRs of the $Fe_{48}Cr_{15}Mo_4Er_2C_{15}B_6$ BMG in 1 N HCl, 1 N NaOH, and 0.6 M NaCl solutions are 39.9, 27.5, and 3 μm/year, respectively. Fig. 2a give the CPRs of the different BMG materials and stainless steel in 0.6 M NaCl. The CPR of the stainless steel is about 1.5 μm/year, which is the same order of magnitude with the $Fe_{48}Cr_{15}Mo_4Er_2C_{15}B_6$ BMG. Fig. 2b gives the CPR of the Cu-based BMGs and $Fe_{48}Cr_{15}Mo_4Er_2C_{15}B_6$ BMG. The CPR of $Fe_{48}Cr_{15}Mo_4Er_2C_{15}B_6$ BMG is significantly lower than those of Cu-based BMG. Not very many results were reported in 1 N NaOH, thus, the comparing figure in NaOH is not given in this paper. The low CPRs of $Fe_{48}Cr_{15}Mo_4Er_2C_{15}B_6$ BMG suggest very good corrosion properties, comparing with other materials.

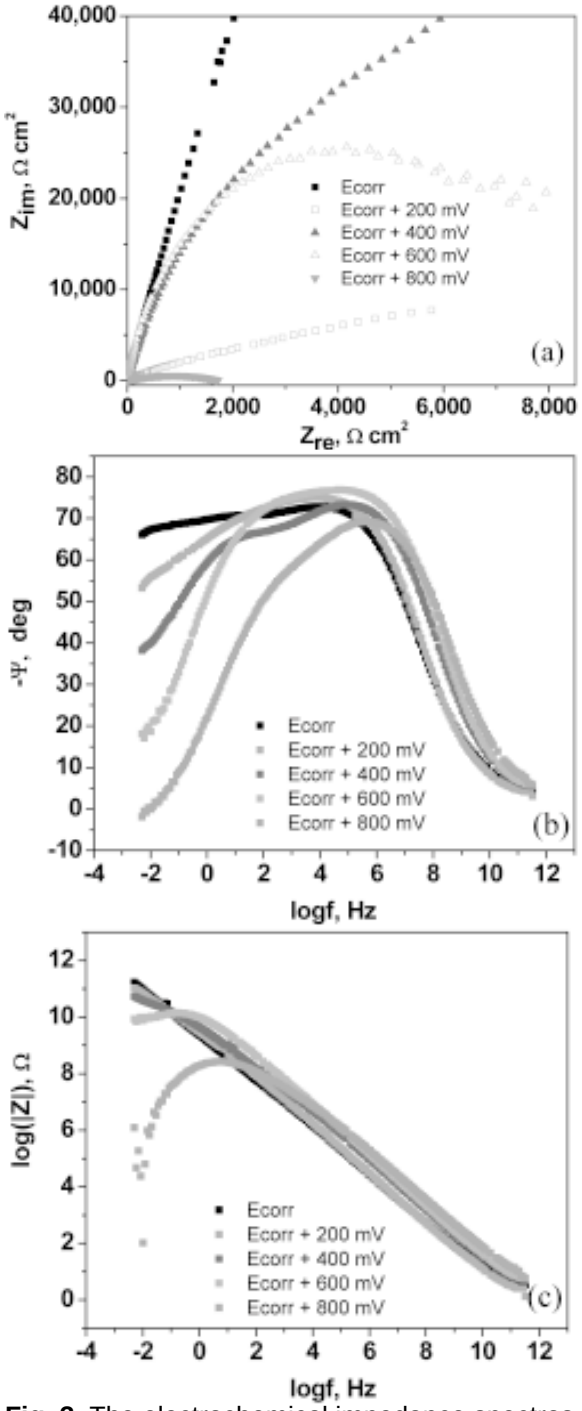

Fig. 3. The electrochemical impedance spectroscopy of $Fe_{48}Cr_{15}Mo_4Er_2C_{15}B_6$ BMG in 0.6 M NaCl solution, (a) Nyquist figure, (b) Bode figure ψ versus logf, and (c) Bode figure log|*Z*| versus log*f*.

3.2. Electrochemical-Impedance-Spectroscopy (EIS)

The detailed information about the corrosion behavior of $Fe_{48}Cr_{15}Mo_4Er_2C_{15}B_6$ BMG is drawn from

the EIS, exemplified by the corrosion in the 0.6 M NaCl solution. The arc in Nyquist diagram is a part of a circle. The coordination of the circle center (x,y) is [R_a/2,R_a/2ctg($n\pi$/2)], and the radius of the circle is R_a/4sin($n\pi$/2), where R_a is the resistance of the electrode, and n is the power of Z [$Z = (j\omega)^{-n}/Y_0$] [15,16]. The Nyquist diagrams at different passive potentials are shown in Fig. 2a. According to the Nyquist diagram, the resistance of the electrode decreases from $E_{corr.}$ to $E_{corr.}$ + 200 mV, then increases to $E_{corr.}$ + 400 mV, after that decreases again up to $E_{corr.}$ + 800 mV. The changing trend of the resistance of the electrode is in agreement with the polarization curve. The first decrease of the electrode resistance corresponds to the dissolution of the anode, and the increase of the electrode resistance shows the formation of the passive film. Then, the second decrease of the electrode proves the occurrence of the pitting.

Figs. 3b and 3c describe the Bode figures at different passive potentials. The maximum phase (Ψ) in Fig. 3b corresponds to the electron-transfer rate. The greater maximum phase means a lower electron-transfer rate, revealing a larger resistance. The lowest point in Fig. 3c corresponds to the resistance of the solution. The highest point corresponds to the resistance of the solution, and the electrode. From the $E_{corr.}$, both the maximum phase in the Ψ versus log$f$ figure and the highest point in the log|Z| versus log$f$ figure decrease, then increase, and decrease again, which also correspond to the dissolution of the electrode, the formation of the passive film, and the destabilization of the passive film, respectively. The changing trend is in agreement with the results of the Nyquist figures and the polarization curves as discussed in the previous paragraph.

4. CONCLUSIONS

1. The CPRs of $Fe_{48}Cr_5Mo_4Er_2C_{15}B_6$ BMG in 1 N HCl, 1 N NaOH, and 0.6 M NaCl with pH of 7 solutions are 39.9, 27.5, and 3 mm/year, respectively, indicating very good corrosion properties in different environments, compare with other materials.
2. The polarization curves include the dissolution of the anode, the formation of the passivation films, and the transpassive or pitting phenomenon. The Nyquist and Bode figures give the change of the resistance of the electrode, which is in good agreement with the variation of the polarization curve.

ACKNOWLEDGEMENTS

This work was supported by the National Science Foundation Combined Research-Curriculum Development (CRCD) Program with Ms. M. Poats as the Program Director, under EEC-9527527 and EEC-0203415. We would like to thank Drs. S. J. Poon, G. J. Shiflet, and V. Ponnambalam of University of Virginia for their kind help.

REFERENCES

[1] A. Inoue, B.L. Shen, A.R. Yavari and A.L. Greer // *J. Mater. Res.* **18** (2003) 1487.
[2] V. Ponnambalam, S.J. Poon, G.J. Shiflet, V.M. Keppens, R. Taylor and G. Petculescu // *Appl. Phys. Lett.* **83** (2003) 1131.
[3] A. Inoue, T. Zhang and A. Takeuchi // *Appl. Phys. Lett.* **71** (1997) 464.
[4] V. Ponnambalam, S. J. Poon and G. J. Shiflet // *J. Mater. Res.* **19** (2004) 1320.
[5] Z.P. Lu, C. T. Liu and P. Thompson // *Phys. Rev. Lett.* **92** (2004) 245503.
[6] V. Ponnambalam, S. J. Poon and G. J. Shiflet // *J. Mater. Res.* **19** (2004) 3046.
[7] M. L. Morrison, R. A. Buchanan, A. Peker, W. H. Peter, J. A. Horton and P. K. Liaw // *Intermetallics* **12** (2004) 1177.
[8] W. H. Peter, P. K. Liaw, R. A. Buchanan, C. T. Liu, C. R. Brooks, J. A. Horton, C. A. Carmichael and J. L. Wright // *Intermetallics* **10** (2002) 1125.
[9] M. L. Morrison, R. A. Buchanan, O. N. Senkov, D. B. Miracle and P. K. Liaw // *Metall. and Mater. Trans. A* **37** (2006) 1239.
[10] M. L. Morrison, R. A. Buchanan, P. K. Liaw, C. J. Berry, R. L. Brigmon, L. Riester, H. Abernathy, C. Jin and R. J. Narayan // *Diam. Relat. Mater.* **15** (2006) 138.
[11] M. L. Morrison, R. A. Buchanan, R. V. Leon, C. T. Liu, B. A. Green, P. K. Liaw and J. A. Horton // *J. Biomed. Mater. Res. A* **74A** (2005) 430.
[12] E.E. Stansbury and R.A. Buchanan, *Fundamentals of electrochemical corrosion* (ASM International, Materials Park, OH, 2000).
[13] R. Vandenkerchhove, M. Chandrasekaran, P. Vermaut, R. Portier and L. Delaey // *Materials Science and Engineering A* **378** (2004) 532.
[14] K. Asami, C. L. Qin, T. Zhang and A. Inoue // *Materials Science and Engineering A* **375** (2004) 235.

[15] F. X. Qin, H. F. Zhang, Y. F. Deng, B. Z. Ding and Z. Q. Hu // *Journal of Alloys and Compounds* **375** (2004) 318.

[16] S. A. Yuan and S. S. Hu // *Electrochimica Acta* **49** (2004) 4287.